Rare Metal Materials and Engineering
Volume 52, Issue 2, February 2023
Available online at www.rmme.ac.cn

Science Press

Cite this article as: Gong Yuan, He Junguang, Wen Jiuba, et al. Effect of Hot Extrusion on Microstructure and Properties of As-cast Mg-1Zn-0.3Zr-1Y-2Sn Magnesium Alloy[J]. Rare Metal Materials and Engineering, 2023, 52(02): 508-516.

ARTICLE

Effect of Hot Extrusion on Microstructure and Properties of As-cast Mg-1Zn-0.3Zr-1Y-2Sn Magnesium Alloy

Gong Yuan[1], He Junguang[1,2], Wen Jiuba[1,2], Feng Wuyun[1], Zheng Xiangyang[1], Li Huan[1]

[1] School of Materials Science and Engineering, Henan University of Science and Technology, Luoyang 471023, China; [2] Collaborative Innovation Center of Nonferrous Metals, Luoyang 471023, China

Abstract: The effect of hot extrusion with different extrusion temperatures (340, 360, 380, and 400 °C) on the microstructure evolution and properties of the as-cast Mg-1Zn-0.3Zr-1Y-2Sn magnesium alloy was investigated by optical microscopy (OM), scanning electron microscopy (SEM), immersion experiments, electrochemical experiment, and tensile test. The results show that after hot extrusion, the second phase of the alloy is broken into particles along the extrusion direction, while the grain size is significantly reduced, and dynamic recrystallization and deformation grains exist in the microstructure. As the extrusion temperature increases, the content of the second phase changes less, and the size of the dynamic recrystallization grain gradually increases. The mechanical properties of the extruded alloys are improved, but their corrosion resistance is weakened. The hot extrusion treatment can improve the corrosion resistance of the alloy in the early stage of corrosion, while as the corrosion proceeds, the corrosion resistance of the alloy in the later stage is weakened. When the hot extrusion temperature is 360 °C, the extruded alloy has relatively good mechanical properties and corrosion resistance.

Key words: magnesium alloy; hot extrusion; corrosion resistance; mechanical properties

As a degradable biomaterial, magnesium alloys have good biocompatibility and application prospects in the field of bone repair[1–4]. However, there are some problems in magnesium alloys research: (1) the biocompatibility and safety of magnesium alloys need to be clarified[1]; (2) their mechanical properties, especially the plasticity, need to be improved[5–7]; (3) the standard electrode potential of magnesium is too low and the oxide film on the magnesium alloy surface is porous structure, making magnesium alloys prone to corrosion in vitro and in vivo[8]. Matching between the mechanical properties and corrosion resistance of magnesium alloy becomes a key issue for the development and application of biodegradable magnesium alloys.

At present, the methods to improve the mechanical properties and corrosion resistance of magnesium alloys mainly include alloying, heat treatment, hot deformation, and surface treatment. Among them, alloying and hot extrusion treatments are more widely used. In terms of alloying, Zn is a common alloying element, which can effectively improve the mechanical properties and corrosion resistance of the magnesium alloy[9]. Zr element can refine the grains of the magnesium alloys, reduce the brittleness and improve the strength of the alloys[10–11]. In addition, Y element is helpful to improve the mechanical properties and corrosion resistance of the magnesium alloys[12–13]. Furthermore, the addition of Sn element in magnesium alloy can form the Mg_2Sn phase with high thermal stability, which facilitates the grain refinement and helps to improve the mechanical properties of the magnesium alloys[14–16].

The ideal biodegradable materials should have the following characteristics: (1) good biocompatibility and degradability; (2) degradation products are harmless; (3) high strength; (4) degradation rate and the performance of the cell function match well; (5) the material can guide or induce tissue regeneration[17–21]. Generally, the microstructure of as-cast magnesium alloy is not uniform. The large grain size of the alloy and composition bias in the microstructure are not conducive to the development of the mechanical properties

Received date: September 02, 2022
Foundation item: Supported by Henan Key Laboratory of Non-ferrous Materials Science and Processing Technology
Corresponding author: He Junguang, Ph. D., Professor, School of Materials Science and Engineering; Henan University of Science and Technology, Luoyang 471023, P. R. China, E-mail: he.ellen@163.com

and corrosion resistance of the as-cast alloy[22–23]. Hot extrusion is an important method to improve the microstructure and properties of the magnesium alloys, which can produce a refined and uniform microstructure to obtain higher strength and plasticity[24–26]. Besides, hot extrusion also has an important effect on the corrosion resistance of magnesium alloys. Zhang et al[27] studied the effect of hot extrusion speeds on the microstructure and properties of as-cast Mg-3Zn-1Y-0.6Zr-0.5Ca alloy. They found that dynamically recrystallized grains form in the alloy after hot extrusion, and with the increase in the hot extrusion speed, the size of the dynamic recrystallized grain and the plasticity of the alloy gradually increase, while the ultimate tensile strength (UTS) gradually decreases. Yang et al[28] compared the corrosion behavior of Mg-Sn-Y alloy before and after hot extrusion and found that the hot extrusion can increase the corrosion rate of Mg-Sn-Y alloy. In contrast, Abuleil et al[29] found that hot extrusion can reduce the corrosion rate of Mg-Sn-Ca alloy and improve its corrosion resistance.

According to the present research, hot extrusion can improve the mechanical properties of magnesium alloys, but its effects on the corrosion resistance of the alloys are still uncertain[30–31]. Therefore, in this research, a novel as-cast Mg-1Zn-0.3Zr-1Y-2Sn (wt%) alloy was treated by hot extrusion at different extrusion temperatures, and the effects of extrusion temperature on the microstructure, mechanical properties, and corrosion behavior of the alloy were studied.

1 Experiment

1.1 Alloy preparation

Commercially pure Mg (99.95%), pure Zn (99.99%), Mg-30wt% Zr, Mg-20wt% Y, and Mg-20wt% Sn master alloys were used to prepare the as-cast Mg-1Zn-0.3Zr-1Y-2Sn alloys. The melting was performed in a vacuum induction melting furnace (ZGJL0.01-40-4) under a protective gas of CO_2 (99vol%) and SF_6 (1vol%). The melting temperature was 750 ° C and the casting temperature was 720 ° C. Before casting, the mold was preheated to 200 ° C. After that, the ingots were cut into a billet of *Φ*49 mm×36 mm. Hot extrusion was conducted at 340, 360, 380, and 400 °C, with an extrusion ratio of 10:1 and an extrusion rate of 5 mm/min. The size of the billet after the hot extrusion treatment was *Φ*16 mm×260 mm.

1.2 Microstructural analysis

The microstructures of the as-cast alloy and the extruded alloys in the parallel extrusion direction were observed by optical microscope (OM), and the corrosive agent was the picric acid solution, whose main components were 4.5 g picric acid+100 mL anhydrous ethanol+9 mL deionized water+5 mL glacial acetic acid. The grain sizes of the alloys were measured by Nano-Measurer software. The morphologies and composition of the second phase of the alloys were characterized by scanning electron microscope (SEM, JSM-5610LV) equipped with energy-dispersive spectrometer (EDS).

1.3 Tensile test

The mechanical properties of the tensile specimen parallel to the extrusion direction were measured at room temperature by an electronic universal testing machine (DNS100). Based on the GB/T228.1-2010 standard, the tensile specimens were processed into the ones with 54.11 mm in length, 3.1 mm in width, 2 mm in thickness, and 15 mm in scale distance. The tensile rate was 1 mm/min. Three specimens were selected for each group of experiments, and the average value was calculated. The fracture morphology of the specimens after stretching was observed by SEM.

1.4 Immersion tests

The mass-loss corrosion test sample was parallel to the extrusion direction, the size of the sample was *Φ*14 mm×5 mm, the corrosion solution was simulated body fluid (SBF), and the main components of the SBF were: 8 g/L NaCl, 1 g/L glucose, 0.06 g/L $MgSO_4·7H_2O$, 0.06 g/L KH_2PO_4, 0.06 g/L Na_2HPO_4, 0.35 g/L $NaHCO_3$, 0.14 g/L $CaCl_2$, 0.4 g/L KCl, 0.1 g/L $MgCl_2·6H_2O$. According to the ASTM-G01-03 standard, the ratio of SBF volume (mL) to specimen area (cm^2) was 30:1. The temperature of SBF was controlled at 37±0.5 °C by a water bath, and the corrosion time was 120 h. The SBF was replaced every 24 h. The corrosion products were removed by boiled chromic acid solution (3 g $AgNO_3$+60 g chromic acid+300 mL deionized water). An electronic analytical balance with an accuracy of 0.1 mg was used to weigh the mass loss. The mass-loss corrosion rate was calculated by Eq.(1):

$$V=KW/AT\rho \quad (1)$$

where K is the time conversion factor (K=8.76×10^4), W is the mass loss after corrosion (g), A is the area of the specimen exposed to the solution (cm^2), T is the immersion time (h), and ρ is the density of the material (g/cm^3). Three specimens were selected for each group of experiments and their average values were calculated. The corrosion morphologies were observed by SEM.

Specimen with sizes of *Φ*11.3 mm×8 mm were selected for the hydrogen evolution experiment. First, the sample was ground and polished, ultrasonically cleaned with acetone and alcohol for 2 min, and then placed in a 150 mL beaker of SBF at 37 ° C. The data was recorded every 24 h, the immersion time was from 0 h to 120 h and the SBF was replaced every 24 h. Three specimens were selected for each group of experiments and their average values were calculated.

The electrochemical corrosion properties of the alloys were tested using an electrochemical workstation. A standard three-electrode system was used, in which the specimen was the working electrode (test area of 1 cm^2), graphite flake was the auxiliary electrode, and saturated glycerol electrode was the reference electrode. The specimens were immersed in SBF at 37 ° C for 3600 s to test their open circuit potential (OCP). Then the electrochemical impedance (EIS) was tested on this basis with the following main parameters: amplitude of 5 mV and frequency range from 10^5 Hz to 10^{-1} Hz.

2 Results and Discussion

2.1 Microstructure analysis

Fig. 1 and Fig. 2 show the microstructure and grain size distribution of Mg-1Zn-0.3Zr-1Y-2Sn alloy with different treatments. It can be seen that the microstructure of the as-cast alloy is mainly dendrite (Fig. 1a). After hot extrusion (Fig. 1b–1e), the dendrite disappears, and the extruded alloy has a bimodal microstructure, i. e. equiaxed dynamic recrystallized grains and deformed grains elongated along the extrusion direction. The appearance of dynamic recrystallization indicates that the alloy undergoes dynamic recrystallization during hot extrusion. As the extrusion temperature increases from 340 ° C to 400 ° C, the proportion of dynamic recrystallization grain increases, its average grain size increases from 14 μm to 30 μm, and the grain distribution becomes more inhomogeneous. On the contrary, the proportion of deformed grains gradually decreases and twinning appears in the grains. The proportion of dynamically recrystallized grains in the microstructure gradually increases with the increase in extrusion temperature, indicating that the increase in temperature can promote the dynamic recrystallization. The main reasons are as follows: (1) the increase in temperature can accelerate the coordinated deformation process between grains and avoid the formation of deformed grains[32–33]; (2) the increase in temperature can reduce the movement resistance of dislocations and grain boundaries, and promote the growth of dynamically recrystallized grains[34]. When the extrusion temperature is 360 °C, the grain distribution of dynamic recrystallization in the alloy is relatively uniform, and its average grain size is 15 μm.

Fig. 3 shows the SEM images of the alloys with different treatments. It can be seen that the second phase in the as-cast alloy is elongated and granular, mainly distributed at the grain boundaries (Fig. 3a). After hot extrusion (Fig. 3b – 3e), the second phase is broken into granular shapes and distributed along the extrusion direction. As the extrusion temperature increases, the content, size, and distribution of the second phase in the extruded alloys do not change significantly, which indicates that the influence of extrusion temperature on the second phase is not obvious. The results of the EDS analysis for the second phase are shown in Table 1. It can be seen that the second phase is mainly composed of Mg, Sn, and Y elements. After hot extrusion treatment, the atomic ratio of Sn: Y elements in the second phase is about 1: 1, so it can be presumed that the second phase is mainly the MgSnY phase.

2.2 Mechanical properties

Fig. 4 shows the mechanical properties of the as-cast alloy and the extruded alloys with different extrusion temperatures. It can be seen that the mechanical properties of the as-cast alloy are significantly improved after the hot extrusion treatment. With the increase in the extrusion temperature from 360 °C to 400 °C, the mechanical properties of the extruded alloys show a trend of increasing first and then decreasing. When the extrusion temperature is 360 °C, the alloy has higher mechanical properties, with yield strength (YS), UTS, and elongation (EL) of 222±12 MPa, 277±10 MPa, and 22.3% ±0.5%, respectively. According to Fig. 1 and Fig. 2, dynamically recrystallized grains and deformed grains with smaller sizes exist in the alloy after hot extrusion, and their influence on the mechanical properties of the alloy is mainly reflected in two aspects: (1) the formation of small dynamically recrystallized grains can improve the strength of the alloy through fine-grain strengthening, and the reduction of grain size can also promote the coordination of deformation between grains and the activation of non-basal plane slip system, which enhances

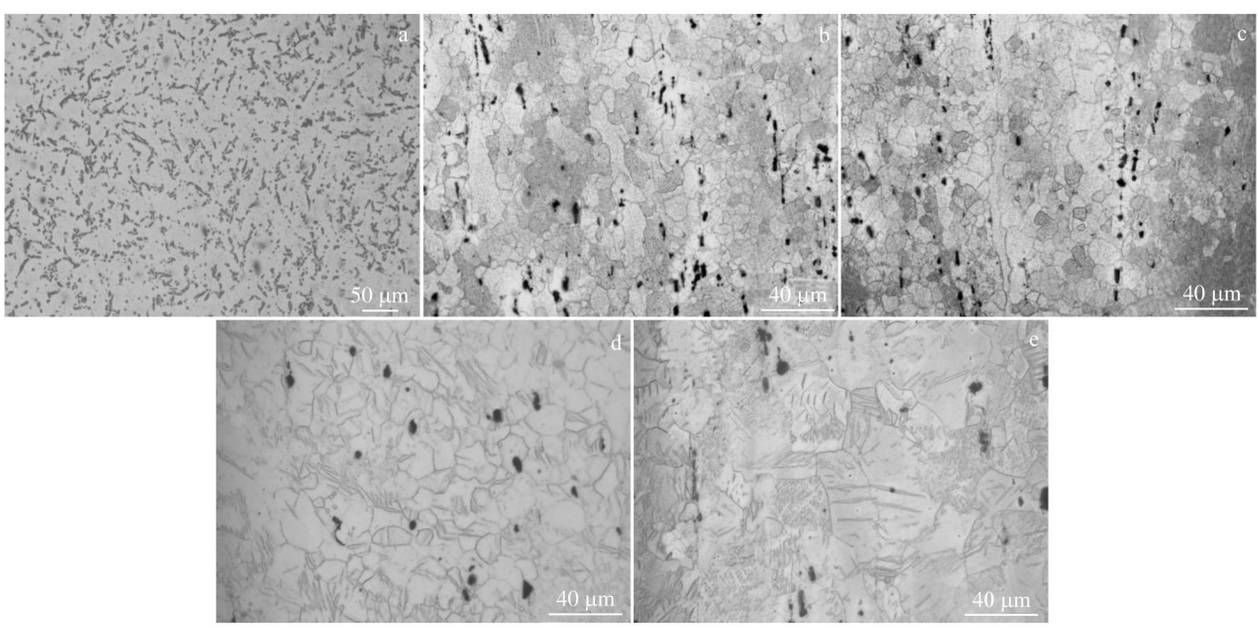

Fig.1 OM microstructures of as-cast alloy (a) and the extruded alloys with different extrusion temperatures: (b) 340 °C, (c) 360 °C, (d) 380 °C, and (e) 400 °C

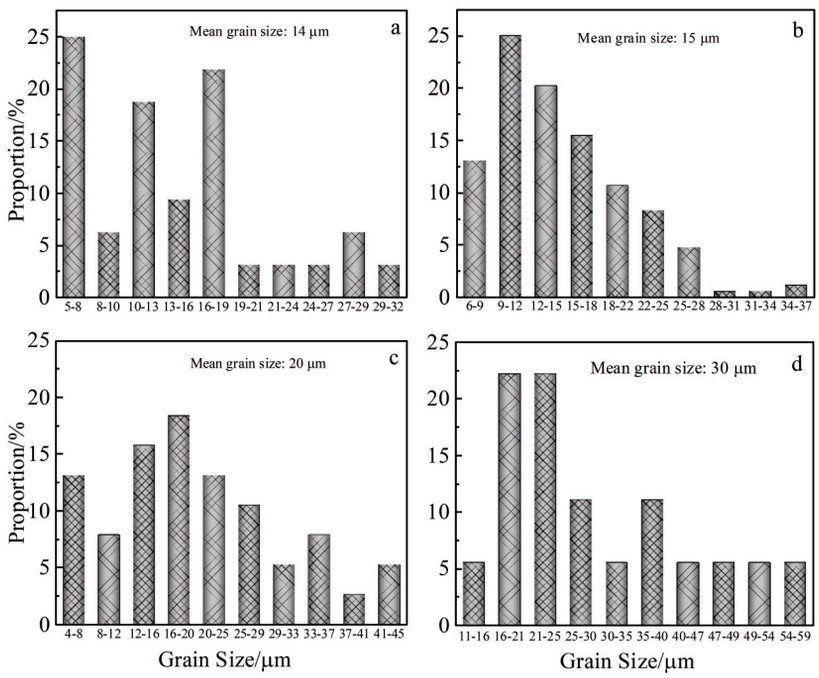

Fig.2 Grain size distribution of the extruded alloys with different extrusion temperatures: (a) 340 °C, (b) 360 °C, (c) 380 °C, and (d) 400 °C

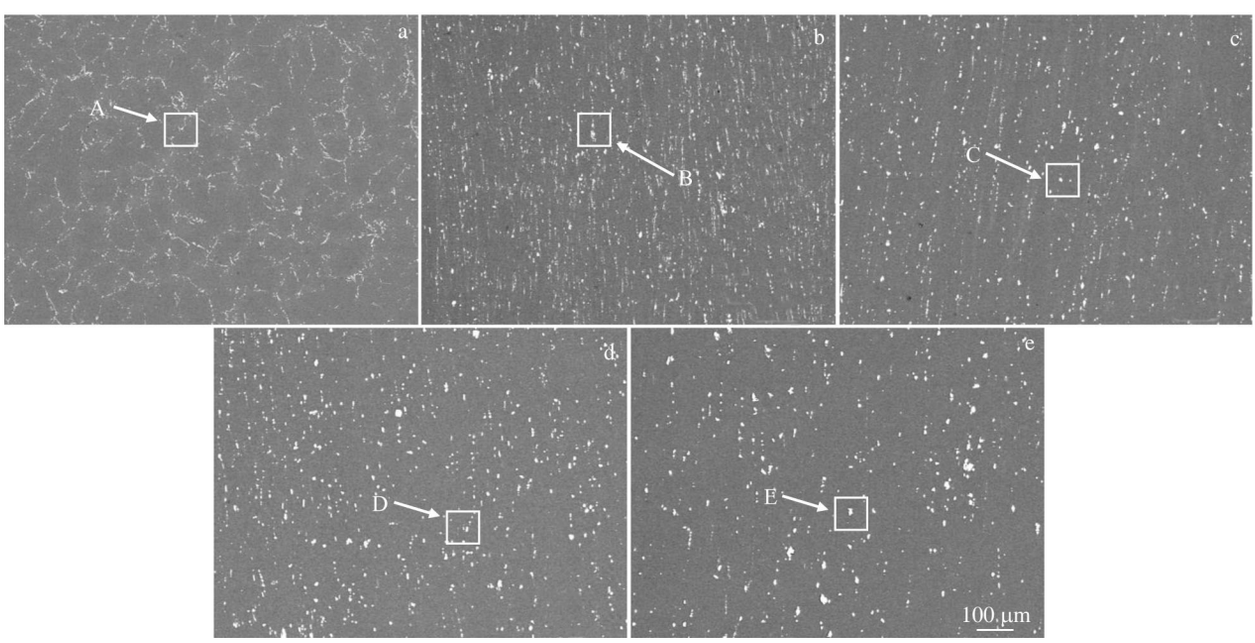

Fig.3 SEM images of as-cast alloy (a) and the extruded alloys with different extrusion temperatures: (b) 340 °C, (c) 360 °C, (d) 380 °C, and (e) 400 °C

Table 1 EDS analysis results of the second phases marked in Fig.3

Position	Element content/wt%			Element content/at%			Sn/Y
	Mg	Sn	Y	Mg	Sn	Y	
A	52.23	29.26	18.5	82.53	9.47	8	1.18
B	81.43	11.47	7.10	94.99	2.74	2.27	1.20
C	71.42	15.98	12.60	91.40	4.19	4.41	0.95
D	64.30	19.18	16.51	88.39	5.40	6.21	0.87
E	63.50	22.33	14.17	88.26	6.36	5.38	1.18

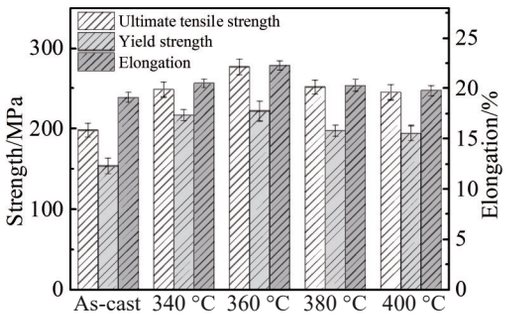

Fig.4 Mechanical properties of as-cast alloy and extruded alloys with different extrusion temperatures

the alloy plasticity[35–36]; (2) deformed grains are not conducive to the slip of dislocations, increasing the strength of the alloy but reducing the ductility of the extruded alloys[37]. With the increase in extrusion temperature, the size of dynamically recrystallized grains gradually increases, and the proportion of deformed grains decreases, which makes the strength and plasticity of the extruded alloys increase first and then decrease.

Fig. 5 shows the fracture morphologies of the as-cast alloy and the extruded alloys with different extrusion temperatures. From Fig. 5a, it can be seen that the fracture morphology of the as-cast alloy has cleavage planes with a large size, obvious tear ridges, and a small number of dimples, which exhibit a quasi-destructive fracture mechanism. After hot extrusion, as shown in Fig. 5b – 5e, the fracture profiles of the extruded alloys show a significant reduction in the size of the cleavage planes compared with that of the as-cast alloy, but the number of tear ridges and dimples increases significantly, showing a certain degree of plasticity. According to the fracture morphologies, all the extruded alloys with different extrusion temperatures are quasi-destructive fracture mechanisms.

2.3 Corrosion behavior

Fig. 6 shows the corrosion rate of the as-cast alloy and the extruded alloys with different extrusion temperatures after immersion in SBF for 120 h. It can be seen that after the hot extrusion treatment, the corrosion rate of the extruded alloy increases compared with that of the as-cast alloy, and the corrosion rates of the extruded alloys show a trend of decreasing first and then increasing with increasing the extrusion temperature. When the extrusion temperature is 360 °C, the corrosion rate of the extruded alloy is the lowest with a value of 1.37±0.06 mm/a, which is similar to that of the as-cast alloy.

Fig. 7 shows the variation curves of hydrogen precipitation of the as-cast alloy and the extruded alloys with different extrusion temperatures after immersion in SBF from 0 h to 120 h. It can be seen that the hydrogen evolution volume increases first sharply and then gradually slowly with the corrosion proceeding. The main reason is as follows: the strong chemical activity of magnesium leads to rapid reaction on the surface in contact with the corrosion solution to generate H_2, resulting in a rapid increase in the hydrogen evolution volume. As the corrosion proceeds, the corrosion products formed on the surface of the alloy cover the surface of the alloy, which hinders the corrosion process and slows down the increasing rate of the hydrogen evolution volume[38]. When the extrusion temperature is 360 °C, the variation of hydrogen evolution volume of the extruded alloy is relatively small, indicating that the alloy has relatively good corrosion resistance.

Fig.8 shows the corrosion morphologies of the as-cast alloy

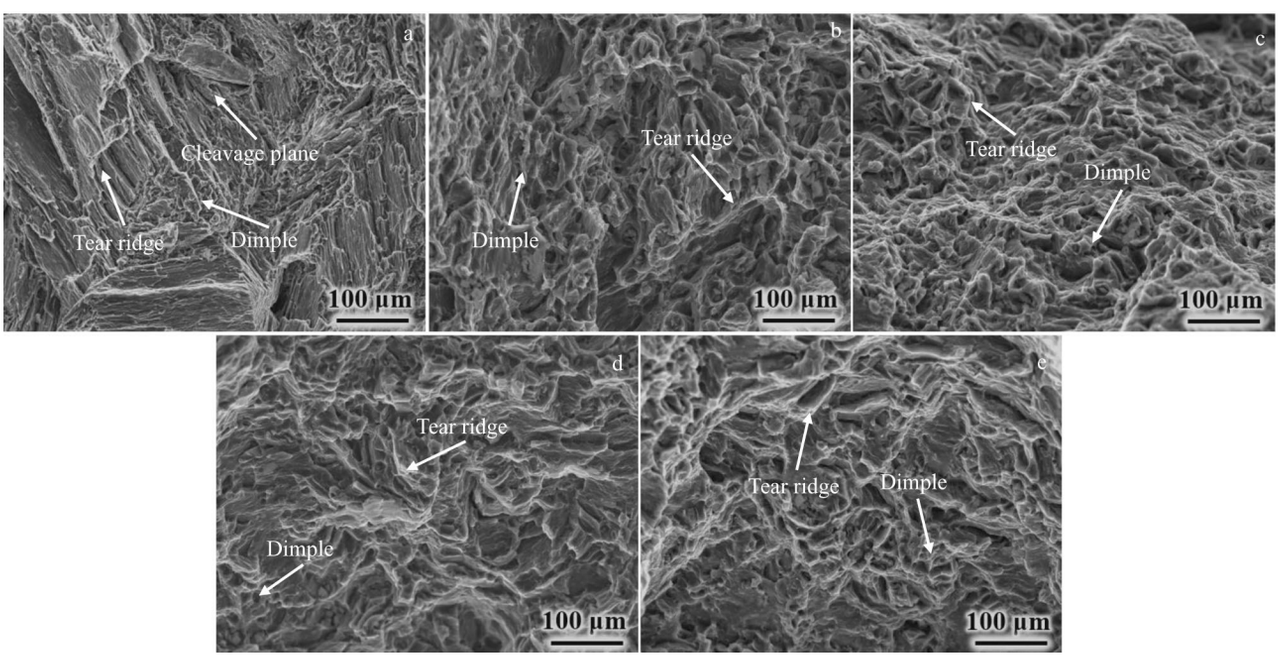

Fig.5 Fracture morphologies of as-cast alloy (a) and extruded alloys with different extrusion temperatures: (b) 340 °C, (c) 360 °C, (d) 380 °C, and (e) 400 °C

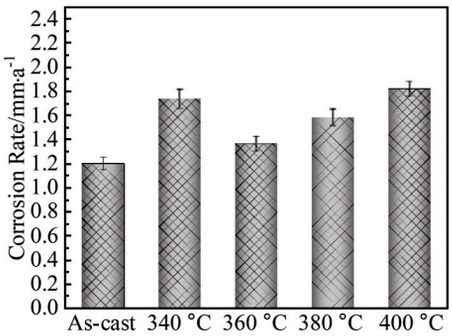

Fig.6 Corrosion rates of the as-cast alloy and the extruded alloys with different extrusion temperatures after immersion in SBF for 120 h

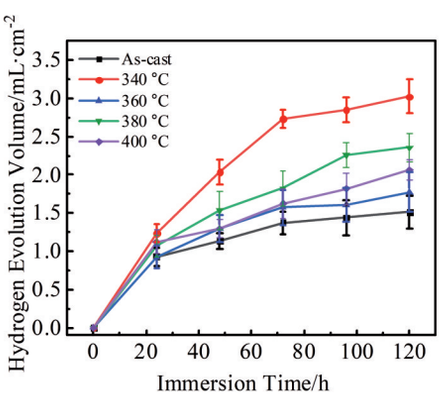

Fig.7 Hydrogen evolution curves of as-cast alloy and extruded alloys with different extrusion temperatures after immersion in SBF from 0 h to 120 h

and the extruded alloys with different extrusion temperatures in SBF for 120 h. It can be seen that before the hot extrusion treatment, many cluster corrosion products appear on the surface of the as-cast alloy. After the alloy is subjected to hot extrusion treatment, the corrosion products on the surface of the extruded alloy are increased compared with that of the as-cast alloy. Among them, when the extrusion temperature is 360 °C, the corrosion products on the surface of the alloy are relatively few, indicating that the corrosion degree of the alloy is relatively slight.

Fig. 9 shows the corrosion morphologies of the alloys after immersion in SBF for 120 h without corrosion products. It can be seen that there are many pitting holes and filiform corrosion morphologies on the corrosion surface of the as-cast alloy. After hot extrusion at different extrusion temperatures, the number of pitting holes on the surface of the extruded alloys is reduced compared to that of the as-cast alloy, and the corrosion morphologies are mainly the filiform corrosion for the extruded alloys. Among them, when the extrusion temperature is 360 °C, the corrosion degree of the alloy is the slightest.

The main reason for the weakened corrosion resistance of the alloys after hot extrusion is that the hot extrusion causes the second phase in the as-cast alloy to break into granular shapes[39–40]. In the process of galvanic corrosion, the second phase is rich in Sn and Y elements, and its electrode potential is higher than that of the Mg matrix, so the second phase acts as the cathodic phase, while the Mg matrix acts as the anodic phase and gradually dissolves[41–42]. With the gradual dissolution of the Mg matrix near the second phase, the granular second phase has a larger contact area with the corrosion medium than the long second phase and is more easily dislodged from the Mg matrix, making the alloy corrosion rate and hydrogen precipitation increase, as shown in Fig. 6 and Fig. 7. In addition, H_2 precipitation and granular second phase

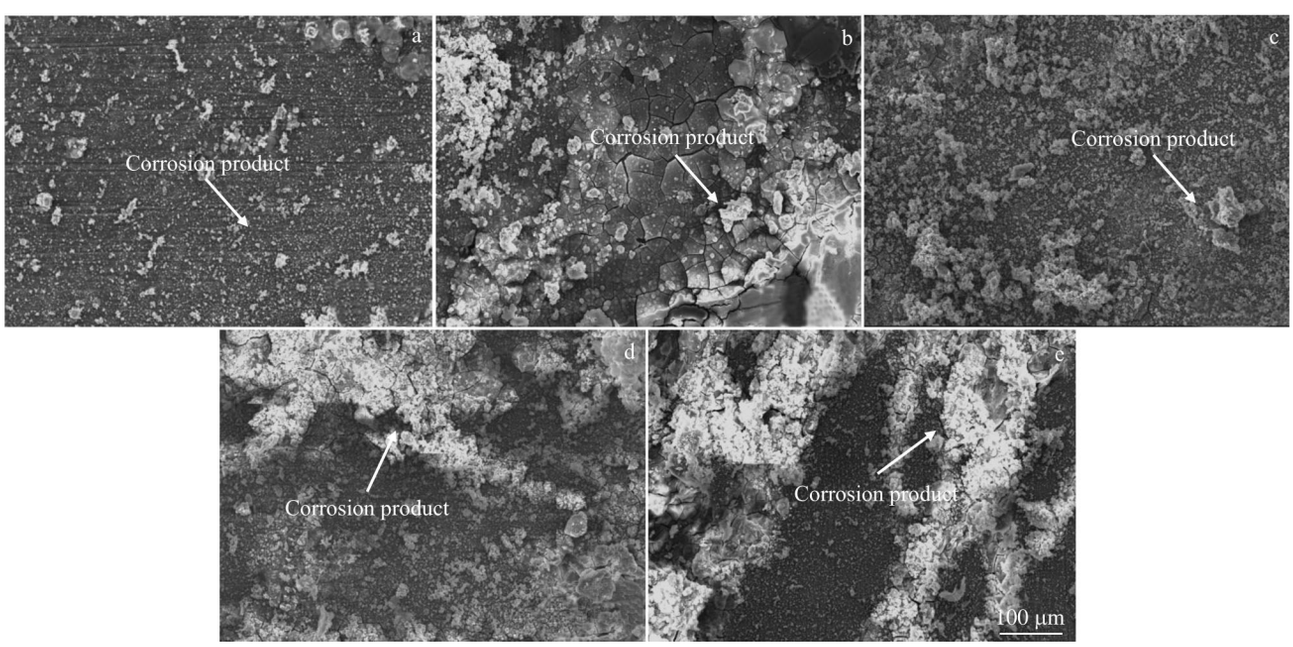

Fig.8 Corrosion morphologies of as-cast alloy (a) and extruded alloys with different extrusion temperatures: (b) 340 °C, (c) 360 °C, (d) 380 °C, and (e) 400 °C

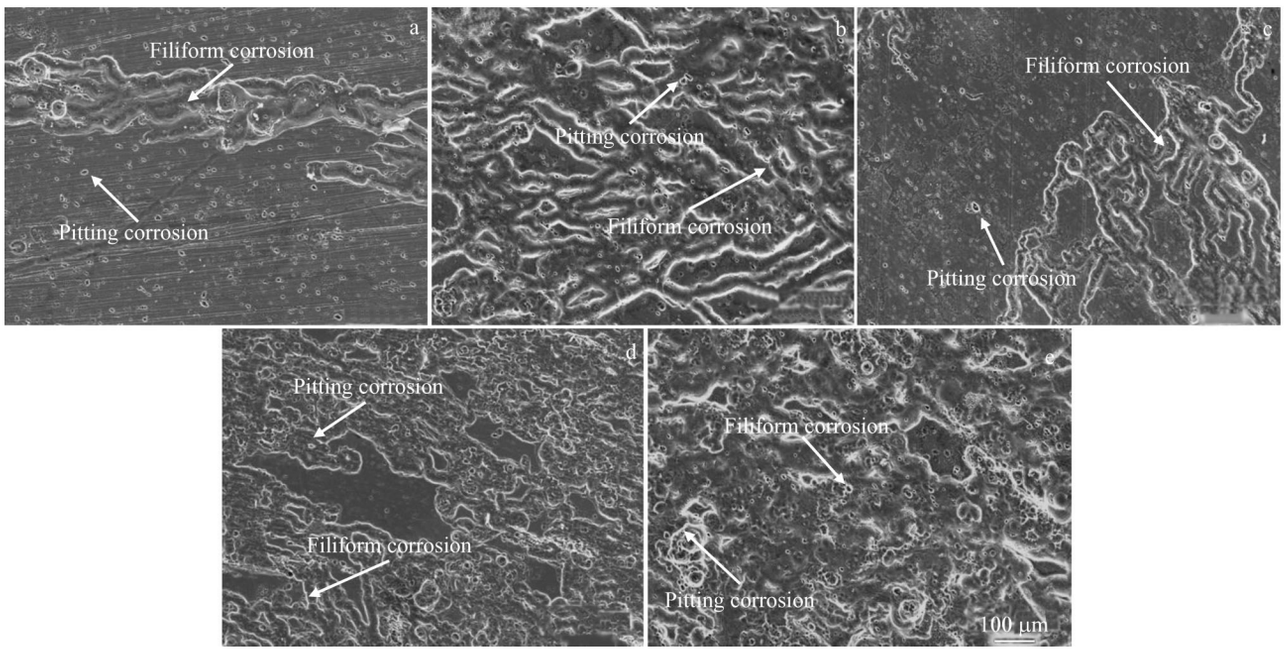

Fig.9 Corrosion morphologies of the as-cast alloy (a) and the extruded alloys with different extrusion temperatures (without corrosion products): (b) 340 °C, (c) 360 °C, (d) 380 °C, and (e) 400 °C

peeling-off will also damage the corrosion layer, accelerating the alloy corrosion process[43–44]. When the extrusion temperature is 360 ° C, the grain size distribution of the extruded alloy is more uniform, and the stress difference in the corrosion layer or protective film formed on surface is smaller. As a result the corrosion layer damage is avoided and the alloy has relatively good corrosion resistance.

Fig. 10 shows the electrochemical impedance spectra and equivalent circuit of the alloys. From Fig. 10a and 10b, it can be seen that the extruded alloys with different extrusion temperatures have larger capacitive arcs and Z values compared with the as-cast alloy, indicating that the extruded alloys have better corrosion resistance than the as-cast alloy. The results differ from the data of mass loss and hydrogen evolution experiments, and the difference is mainly related to the control factors of different corrosion process. Fig. 10d is

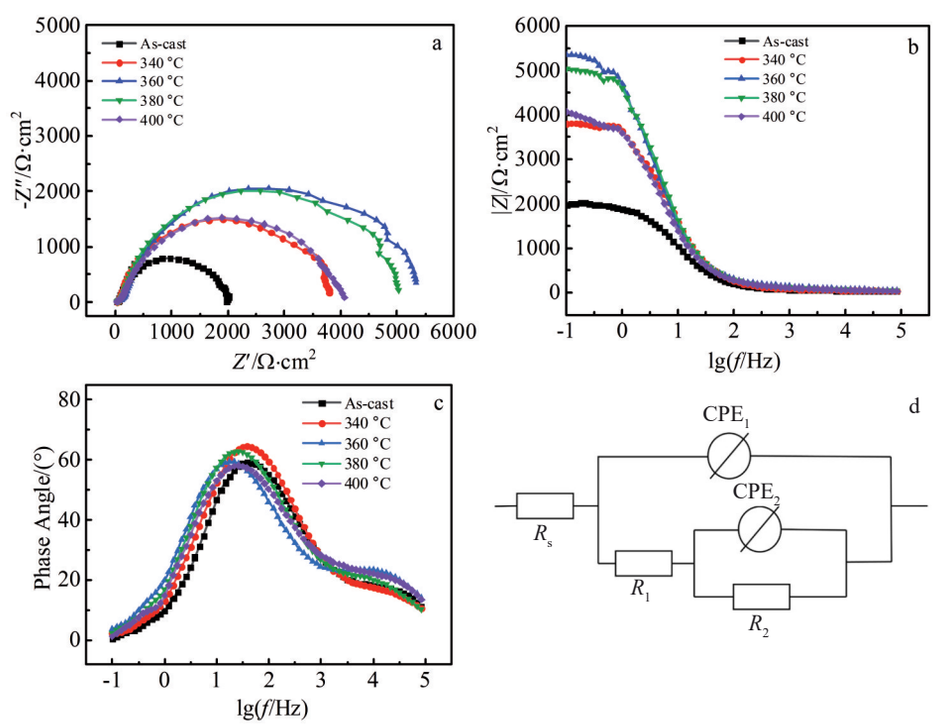

Fig. 10 EIS diagrams and equivalent circuits of as-cast alloy and extruded alloys with different extrusion temperatures: (a) Nyquist diagram, (b, c) Bode diagrams, and (d) equivalent circuits

Table 2 EIS fitting parameters of the as-cast alloy and the extruded alloys with different extrusion temperatures

Temperature/°C	R_s/Ω	CPE_1		R_1/Ω·cm^2	CPE_2		R_2/×10^3 Ω·cm^2
		Y_{01}/×10^{-6} Ω^{-1}·cm^{-2}·s$^{-n_1}$	n_1		Y_{02}/×10^{-5} Ω^{-1}·cm^{-2}·s$^{-n_2}$	n_2	
As-cast	25.12	7.06	0.8	43.27	1.72	0.8	1.97
340	33.71	5.47	0.78	52.97	1.04	0.89	3.78
360	38.78	8.23	0.70	140.4	1.28	0.87	5.44
380	40.08	5.95	0.76	90.74	1.10	0.88	5.06
400	31.62	8.60	0.72	98.32	0.141	0.85	3.99

the equivalent circuit of the alloy corrosion process, where R_s represents the solution resistance, R_1 represents the corrosion layer resistance, R_2 represents the Faraday resistance, CPE_1 and CPE_2 represent the corrosion layer and bilayer constant phase angle elements, respectively. The corresponding fitting data are shown in Table 2. According to Fig.10d and Table 2, it can be seen that the corrosion layer resistance and Faraday resistance of the alloy after hot extrusion are higher than those of the as-cast alloy, indicating that the hot extrusion treatment increases the charge transfer resistance during the corrosion process. This process may be related to the enhanced structural denseness of the corrosion layer or protective film. The hot extrusion treatment can refine the alloy grains and expand the grain boundary area. The chemical activity at the grain boundary is strong, and the enrichment of Zn, Y, Sn, etc at the grain boundary is conducive to the formation of oxide film, which makes the alloy surface form a protective film and hinders the contact between the corrosive medium and the substrate, leading to the enhancement of charge transfer resistance during corrosion.

The above results show that in the early stage of corrosion, hot extrusion treatment can promote the formation of a denser protective film on the surface of the alloy, which plays a major role in corrosion resistance enhancement. With the corrosion proceeding, the structure of the protective film is gradually destroyed, and galvanic corrosion plays a major role in the corrosion resistance of the alloy. Therefore, the hot extrusion treatment can improve the corrosion resistance of the alloy in the early stage of corrosion, and as the corrosion proceeds, the corrosion resistance of the alloy is weakened. In contrast, when the extrusion temperature is 360 °C, the alloy has relatively good corrosion resistance.

3 Conclusions

1) After hot extrusion of the as-cast Mg-1Zn-0.3Zr-1Y-2Sn alloy, the second phase is broken into granular shapes and mainly distributed along the extrusion direction. Dynamically recrystallized and deformed grains exist in the microstructure. With the increase in extrusion temperature, the content, size, and distribution of the second phase change less, the size of dynamically recrystallized grains increases gradually, the distribution is more uneven, and the proportion of deformed grains gradually decreases. When the extrusion temperature is 360 °C, the alloy has a relatively uniform microstructure, and its average grain size of dynamically recrystallized grain is 15 μm.

2) Hot extrusion treatment can significantly improve the mechanical properties of the as-cast alloy. As the extrusion temperature increases from 360 °C to 400 °C, the mechanical properties of the alloy increase first and then decrease. When the extrusion temperature is 360 °C, the alloy has relatively high mechanical property, with YS, UTS, and EL of 222±12 MPa, 277±10 MPa, and 22.3%±0.5%, respectively.

3) The effect of hot extrusion treatment on the corrosion resistance of the alloy is related to the corrosion time. The hot extrusion treatment can improve the corrosion resistance of the alloy in the early stages of corrosion, but it reduces the corrosion resistance of the alloy as the corrosion proceeds. When the extrusion temperature is 360 °C, the alloy has relatively good corrosion resistance, and its corrosion rate after corrosion in SBF for 120 h is 1.37±0.06 mm/a.

References

1 Bowen P K, Drelich J, Goldman J. *Mater Sci Eng C*[J], 2013, 33(8): 5064

2 Wang J, He Y, Maitz M F *et al. Acta Biomater*[J], 2013, 9(10): 8678

3 Gu X N, Zheng Y F. *Front Mater Sci China*[J], 2010, 4(2): 111

4 Zheng Y F, Gu X N, Witte F *et al. Sci Eng R Rep*[J], 2014, 77: 1

5 Xu D, Han E, Xu Y. *Prog Nat Sci Mater Int*[J], 2016, 26(2): 117

6 Liu T, Yang Q, Guo N *et al. J Magnes Alloy*[J], 2020, 8(1): 66

7 Ahmadkhaniha D, Fedel M, Heydarzadeh Sohi M *et al. Surf Eng Appl Electrochem*[J], 2017, 53(5): 439

8 Wang W, Wang Y L, Chen M *et al. Sci Rep*[J], 2016, 6(1): 37 401

9 Doernberg E, Kozlov A, Schmid-Fetzer R. *J Phase Equilibria Diffus*[J], 2007, 6(28): 523

10 Munir K, Lin J, Wen C *et al. Acta Biomater*[J], 2020, 102: 493

11 Cai C, Song R, Wang L *et al. Surf Coat Technol*[J], 2018, 342: 57

12 Qin H, Zhao Y, An Z *et al. Biomaterials*[J], 2015, 53: 211

13 Yu X, Jiang B, Yang H *et al. Appl Surf Sci*[J], 2015, 353: 1013

14 Luo D, Wang H Y, Chen L *et al. Mater Lett*[J], 2013, 94: 51

15 Sasaki T T, Yamamoto K, Honma T *et al. Scr Mater*[J], 2008, 59(10): 1111

16 Sasaki T T, Oh-ishi K, Ohkubo T *et al. Scr Mater*[J], 2006, 55(3): 251

17 Chen Y, Dou J, Yu H *et al. J Biomater Appl*[J], 2019, 33(10): 1348

18 Riaz U, Shabib I, Haider W. *J Biomed Mater Res B Appl*

Biomater[J], 2019, 107(6): 1970
19 Mani G, Feldman M D, Patel D *et al. Biomaterials*[J], 2007, 28(9): 1689
20 Ibrahim H, Esfahani S N, Poorganji B *et al. Mater Sci Eng C*[J], 2017, 70: 870
21 Zreiqat H, Howlett C R, Zannettino A *et al. J Biomed Mater Res*[J], 2002, 62(2): 175
22 Meng S J, Yu H, Fan S D *et al. Engl Lett*[J], 2019, 32(2): 145
23 Song Y, Han E H, Shan D *et al. Corros Sci*[J], 2012, 65: 322
24 Li T, Chai L H, Shi S H *et al. Mater Sci Forum*[J], 2017, 898: 579
25 She J, Pan F, Zhang J *et al. J Alloy Compd*[J], 2016, 657: 893
26 Zhang T, Shao Y, Meng G *et al. Corros Sci*[J], 2011, 53(5): 1960
27 Zhang T, Meng G, Shao Y *et al. Corros Sci*[J], 2011, 53(9): 2934
28 Yang H, Wu L, Jiang B *et al. J Electrochem Soc*[J], 2020, 167: 121 503
29 Abuleil T, Hort N, Dietzel W *et al. Trans Nonferrous Met Soc China*[J], 2009, 19(1): 40
30 Wang B J, Xu D K, Dong J H *et al. Scr Mater*[J], 2014, 88: 5
31 Wang B J, Xu D K, Xin Y C *et al. Sci Rep*[J], 2017, 7(1): 16 014
32 Khorasani F, Emamy M, Malekan M *et al. Mater Charact*[J], 2019, 147: 155
33 Xin Y, Liu C, Zhang X *et al. J Mater Res*[J], 2007, 22: 2004
34 Tian Y, Huang H, Yuan G *et al. J Alloy Compd*[J], 2015, 626: 42
35 Bazhenov V E, Li A V, Komissarov A A *et al. J Magnes Alloy*[J], 2021, 9(4): 1428
36 Zheng K Y, Dong J, Zeng X Q *et al. Mater Sci Eng A*[J], 2007, 454: 314
37 Zhang X B, Yuan G Y, Wang Z Z. *Mater Sci Technol*[J], 2013, 29(1): 111
38 Jin S Y, Ma X C, Wu R Z *et al. Int J Min Met Mater*[J], 2022, 29(7): 1453
39 Ding J, Liu X, Wang Y *et al. Materials*[J], 2019, 12(13): 2069
40 Zeng R, Kainer K U, Blawert C *et al. J Alloy Compd*[J], 2011, 509(13): 4462
41 Ma X C, Jin S Y, Wu R Z *et al. Trans Nonferrous Met Soc China*[J], 2021, 31: 3228
42 Peng Q, Huang Y, Zhou L *et al. Biomaterials*[J], 2010, 31(3): 398
43 Chen J, Wang J, Han E *et al. Corros Sci*[J], 2008, 50(5): 1292
44 Chen J, Dong J, Wang J *et al. Corros Sci*[J], 2008, 50(12): 3610

热挤压对铸态 Mg-1Zn-0.3Zr-1Y-2Sn 镁合金组织和性能的影响

龚　圆[1]，贺俊光[1,2]，文九巴[1,2]，冯武云[1]，郑向阳[1]，李　欢[1]
(1. 河南科技大学 材料科学与工程学院，河南 洛阳 471023)
(2. 有色金属协同创新中心，河南 洛阳 471023)

摘　要：通过光学显微镜（OM）、扫描电镜（SEM）、浸泡实验、析氢实验、电化学试验、拉伸试验等方法，研究了不同挤压温度（340、360、380、400 ℃）下，热挤压对铸态Mg-1Zn-0.3Zr-1Y-2Sn合金组织和性能的影响。结果表明：热挤压后，合金的第二相沿挤压方向破碎成颗粒，微观组织中存在动态再结晶和变形晶粒。随着挤压温度的升高，第二相的含量变化较小，动态再结晶晶粒尺寸逐渐增大。热挤压后，合金的力学性能得到改善，但其耐腐蚀性最终减弱。热挤压处理可以在腐蚀的早期阶段提高合金的耐腐蚀性能，但随着腐蚀的进行，在后期合金的耐蚀性能会降低。当热挤压温度为360 ℃时，合金具有较好的力学性能和耐腐蚀性能。

关键词：生物镁合金；热挤压；耐蚀性能；力学性能

作者简介：龚　圆，女，1998年生，硕士，河南科技大学材料科学与工程学院，河南 洛阳 471023，E-mail：18438605132@163.com